Journal of Manufacturing Processes 39 (2019) 200–207

Contents lists available at ScienceDirect

Journal of Manufacturing Processes

journal homepage: www.elsevier.com/locate/manpro

3D reconstruction of complex spatial weld seam for autonomous welding by laser structured light scanning

Ke Zhang[a,b,*], Minzhi Yan[a,b], Tianyu Huang[a,b], Jian Zheng[a,b], Zhuguo Li[a,b]

[a] Shanghai Key Laboratory of Materials Laser Processing and Modification, Shanghai Jiao Tong University, Shanghai, 200240, China
[b] Collaborative Innovation Center for Advanced Ship and Deep-Sea Exploration, Shanghai, 200240, China

ARTICLE INFO

Keywords:
Laser structured light
Autonomous welding
3D reconstruction
Cubic smoothing spline
Cubic B-spline

ABSTRACT

As to improve the accuracy, efficiency and flexibility of welding process, intelligent welding is an inevitable trend in the future. To realize the modeling of autonomous welding path planning to the spatial complex weld of large workpiece, we designed a weld path autonomous programming system based on laser structure light, which effectively obtained three-dimensional (3D) information of workpiece by multiple segment scanning, then extracted weld features by grayscale image processing, and reconstructed spatial complex curve seam model by cubic smoothing spline and detected characteristic parameters of lap joints, contributing to subsequent self-generated welding procedures. Besides, experimental results showed that the recognition accuracy of the spatial curve seam by proposed method was within 0.4 mm, meeting the weld tracking requirements.

1. Introduction

With the gradual improvement of human cost and the rapid development of information technology in recent years, the application of intelligent welding robot has become an indispensable step in the reform of traditional manufacturing industry and its upgrade into the Industrial 4.0 era. From the microscopic perspective, welding robot can liberate the welding workers in the harsh environment, improve the welding efficiency and quality, and reduce the production cost of enterprises; and from the macroscopic view, recent progresses in the fields of technology, such as sensor and robot technology, big data processing, artificial intelligence, deep learning and so on, have provided some scientific theoretical basis and more potential possibilities for intelligent welding technology, revealing the inevitable trend of digitalization and intellectualization of manufacturing industry in the future [1–10].

However, the intelligent level of widely used welding robot still has a great improvement space. At present, the programming and teaching reproduction welding robot is mainly used in industry, which lacks flexibility and adaptability, and requires high stability of welding environment. In the actual welding production, the machining and assembly error, heat deformation of workpiece in welding process and interference of external forces, causing some deviations between the teaching path and the actual path of weld, affecting the realization of a high automated robotic welding system [1,8]. Generally, an intelligent robotic welding system consist of three basic components [4]: (1) modeling, tracking and profiling of weld seam, (2) welding torch position, orientation control and trajectory planning [11], and (3) welding process parameter control [12–14]. And this study focus on the first component, which is based on one or more kinds of sensing technology to obtain accurate information of welding workpiece and seam, among which visual sensing technology is the most appropriate and promising for its big information quantity, high sensitivity and measurement precision, and non-contact with workpiece, suiting many kinds of groove shapes [8].

Currently, vision sensors applied to welding system are mainly [15] divided into active vision sensor with light source and passive vision sensor under natural light. Many researches of robotic welding system with vision sensor have been proposed in the past decades [16]. Some researchers built passive vision system to realize welding joints recognition [17] or determine the logical tracking point [18,19], but easily affected by noisy environment and existing some recognition error. To get clearer image and improve accuracy of information, many researches for different types of welding conditions [20–27] adopted structured laser as light source for stronger environmental adaptability and anti-interference capability. Therefore, the structured laser vision sensor was used to obtain high quality data of weld seam in this study.

In real-time weld seam tracking, some researchers proposed the method in seam features detection. For instance, Zhu [28] developed a weld deviation detection system based on infrared visual sensing for

* Corresponding author at: Shanghai Key Laboratory of Materials Laser Processing and Modification, Shanghai Jiao Tong University, Shanghai, 200240, China.
E-mail address: zhangke@sjtu.edu.cn (K. Zhang).

https://doi.org/10.1016/j.jmapro.2019.02.010
Received 14 December 2018; Received in revised form 25 January 2019; Accepted 18 February 2019
Available online 28 February 2019

swing arc narrow gap weld tracking, proposed a local pattern recognition algorithm to detect groove edge position, and experimentally investigated their adaptabilities. He [29] also employed a method of autonomously detecting weld seam profiles from molten pool background in metal active gas arc welding using a novel model of saliency-based visual attention. Liu [30] proposed a solution using active contours including an prior for the weld pool boundary composition, and applied Adaboost to select a small set of features that captured the relevant information, realizing weld pool tracking. Fan [31] built an automatic recognition system of welding seam types, and distinguished different welding seam types effectively by feature vector computation and SVM-based modeling method, filtering most of noises from arc lights and splashes and keeping low computation cost. Zou [22,24] designed a set of six-degree-of-freedom robotic welding automatic tracking platform with a three-wire laser vision sensor, proposed the morphological image processing method and CCOT algorithm to detect seam feature points and resolve the issue of strong arc and splash interference, by means of the adaptive fuzzy control algorithm, realizing the real-time tracking of plane complex curve weld seams.

However, real-time tracking not only faces with strong arc and splash interference during welding process, but also requires manual instructional or offline programming before. While another method can avoid welding interference easily and realize autonomous welding with higher efficiency and intelligence, which is sensing the whole seam of workpiece firstly and building the model of the weld seam before welding. Some studies were also employed to recognize seam features before welding. Shah [17] proposed local thresholding approach to automatically recognize and detect the butt welding position for the plane straight, saw tooth and curve joint scenarios using a fixed CCD camera. Chen [32–34] constructed an accuracy analysis model of vision computing based on passive binocular vision sensors fixed on the end effecter of welding robot to compute the position information of spatial seam. However, the modeling of 3D complex curve weld seam has not been mentioned.

As to realize the autonomous welding path planning to the complex weld of large workpiece, and to further improve the intelligence degree of welding operation process, this paper designed a complex weld path autonomous programming system based on laser structure light, which can effectively obtain 3D information of workpiece, reconstruct weld seam and extract characteristic parameters of weld seam, contributing to self-generated welding procedures.

The aim of this paper is to present a new framework for modeling complex weld seam shape using sensor data and conducting automatic path planning thereafter. Firstly, we introduced the experiment, i.e. the robotic welding system (Section 2.1), design for complex seam scanning (Section 2.2). Then, algorithms for preprocessing the image data collected by the laser sensor, reconstructing the shape of the weld seam, and modeling for weld start and end points were discussed (Sections 3.1, 3.2 and 3.3, respectively). Finally, these approaches were validated with experimental results (Section 4), reflecting the reliability of the system.

2. Experiment setup and methods

2.1. Experiment setup for welding

Fig. 1 shows the robotic welding system used in this study. A Motoman SSA2000 6-axis industrial robot, equipped with a Keyence laser displacement sensor (model LJ-G200 with controller model LJ-G5001), is connected to a Yaskawa NX100 robot controller. The robot controller is also connected to a Siemens S7-200 PLC (programmable logic controller) and a computer, which receives the data from controllers of sensor and robot, uploads programs to PLC and robot controller.

When the robot controller drives the robot to scan the workpiece by the sensor, robot controller sends signals to PLC which timing triggers sensor controller to record data simultaneously. Then robot and sensor

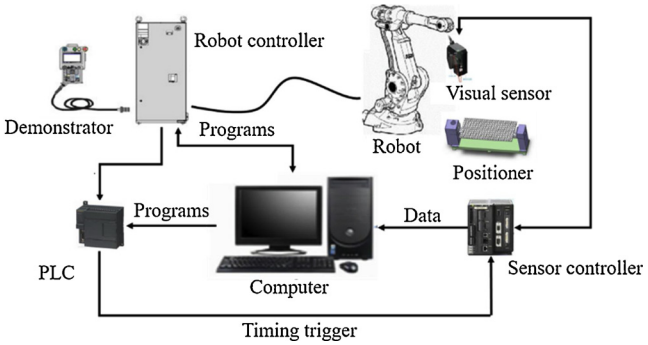

Fig. 1. The robotic welding system platform.

controllers send data to the computer which builds a 3D model of weld seam and a path planning program for robotic welding. The program is uploaded to the robot controller which controls the robot to complete the whole welding process.

2.2. Design for complex seam scanning

To avoid scanning blind area and obtain accurate weld position data as far as possible, this system adopted segmented scanning method for the curve lap welds as shown in Fig. 2. When the robot arrives at the *P1*, the computer synchronously begins to store the data collected by the laser sensor; when it reaches the *P2* point, the computer pauses the storage, the Sensor's internal data is no longer changed, and the number of laser paths collected at this time is recorded *n2*. After the *P2* point pauses, the robot moves to the *P3*, the robot controller outputs the trigger signal again, the computer begins to store the data, and so on until the P6 point ends the data collection. The information in the table is interpolated to indicate the position and posture of the robot corresponding to any scanned laser information stored in the Computer. Assuming that j (number of scanned laser data stored) is greater than ${}^{i}_{m}p$, less than ${}^{i+1}_{m}p$, and the scanning route in between is a straight line, the position and posture of the robot corresponding to the j-th to the laser is:

$$u_j = {}^{i}_{u}p + \frac{{}^{i+1}_{u}p - {}^{i}_{u}p}{{}^{i+1}_{m}p - {}^{i}_{m}p} * (j - {}^{i}_{m}p)\ (u_j = x, y, z, rx, ry, rz;\ i = 1,\ 2...5) \quad (1)$$

3. Modeling

3.1. Data preprocessing

After the hand-eye calibration approach for linear structured light sensors which requires only a reference plate with a straight edge [35], we can obtain 3D point cloud in robot base coordinate system from the 2D sensor output data when the sensor scans along the weld seam (shown in Fig. 3). The point cloud contains the information of spatial locations of the workpiece surface. The preprocessing of these raw data

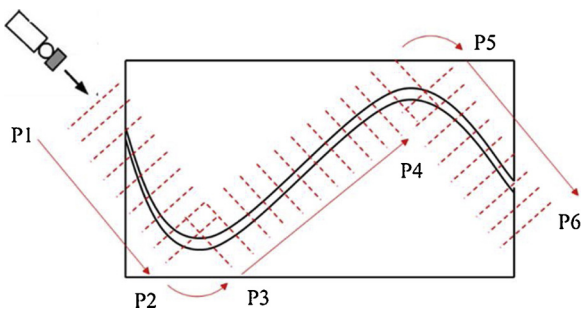

Fig. 2. Design of complex long seam scan path.

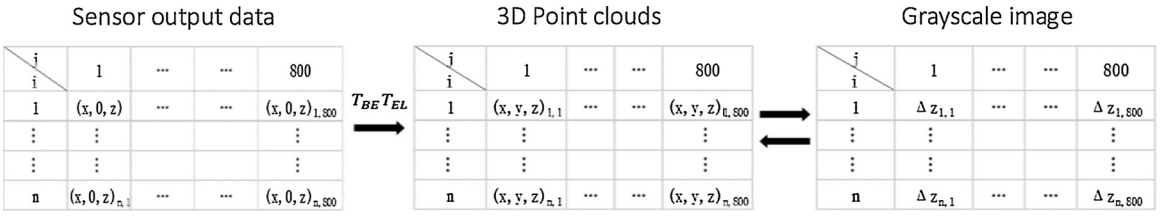

Fig. 3. Conversion relationship between point clouds data and image data.

refers to the filtering and smoothing of the data and identifying the location of the weld seam according to some characteristics. Starting from this section all spatial coordinates are in the robot base coordinate system.

3.1.1. Converting from 3D point cloud to 2D grayscale images

To make the collected data usable by the reconstruction algorithm, it is necessary to convert them from a 3D point cloud to a 2D grayscale image format (shown in Fig. 3). The grayscale value reflects the height change on the location of the pixel, therefore the brighter area (with higher grayscale values) in the image represents the projection of the weld. Let $\{(x_{i,j}, y_{i,j}, z_{i,j})$: $i = 1, ..., m, j = 1, ..., n\}$ be a size m*n point set obtained by taking m measurements and n points per measurement ($n = 800$ in our study), and $\Delta z_{i,j} = |z_{i,j} - z_{i,j-1}|$. The grayscale value on pixel location (i, j), denoted by $I(i, j)$, is defined by $\Delta z_{i,j}$ after min-max normalization then scaled to integer values between 0 and 255:

$$I(i,j) = [\frac{\Delta z_{i,j} - \Delta z_{\min}}{\Delta z_{\max} - \Delta z_{\min}} \cdot 255], \tag{2}$$

where [.] denotes the nearest integer function.

The grayscale image obtained this way (for example, Fig. 4c) does not look exactly the same as the weld seam (shown in Fig. 4a, b), because the pixel coordinate (i, j) are in fact counters for data points instead of the spatial location where the data are sampled. The spatial location information is stored in the base coordinate point set $\{(x_{i,j}, y_{i,j}, z_{i,j})\}$, and we will combine the grayscale image processing result and this information to reconstruct the shape of the weld.

3.1.2. Preprocessing the grayscale image

The purpose of this step is to utilize edge detection algorithms developed by the computer vision community to locate the pixels that represent the weld seam. The preprocessing part involves six steps: grayscale image filtering, image binarization, image smoothing, binary image filtering, edge detection, and fine-tuning. The algorithms applied in each step are summarized in Table 1:

3.2. Spatial reconstruction of curve seam

Section 3.1 describes a method to locate the weld seam from the sensor data. In other words, given the j-th point from the i-th measurement, we know whether it is a weld seam edge point or not. Let $\tilde{I}(i, j)$ denote the processed binary image (Fig. 5f). Note that $\tilde{I}(i, j) = 1$ indicates the weld seam pixels. Therefore $\{(x_{i,j}, y_{i,j}, z_{i,j})$: $\tilde{I}(i, j) = 1\}$ is the set of spatial points of the weld seam. The goal of this step is to fit these points to obtain a smoothing continuous curve from the discrete data, i.e. to reconstruct the shape of the weld seam. Here, two available reconstruction methods are implemented: cubic B-spline and cubic smoothing spline.

Table 1
Image processing algorithms applied to the grayscale image.

Step	Algorithm	Note	Result
Grayscale image filtering	Median filtering	Window size 3×3	Fig. 5a
Image binarization	Otsu thresholding [36]		Fig. 5b
Image smoothing	dilation and Erosion [37]		Fig. 5c
Binary image filtering	Connected domain filtering [38]		Fig. 5d
Edge detection	Canny edge detector [39]		Fig. 5e
Fine-tuning	Zhang-Suen thinning algorithm [40]		Fig. 5f

3.2.1. Cubic B-spline

B-spline is a method to use a piecewise polynomial curve to approximate the nonlinear trend of a dataset. The function is divided by knot points and between the knots the subset of data points is fitted using a carefully-designed polynomial function (spline) such that the global curve satisfies some degree and smoothness requirements. An order *d-1* curve is formed by order d splines defined by:

$$P(x) = \sum_{i=0}^{n} p_i B_{i.d}(x), \quad x_{min} \le x \le x_{max}, \tag{3}$$

where x is the spatial location of a point, p_i are the data points, and $B_{i,d}(\cdot)$ are the spline functions of order *d-1*. They can be derived via the Cox-de Boor recursion formula:

$$B_{i,d}(x) = \frac{x - x_i}{x_i + d - 1 - x_i} B_{i,d-1}(x) + \frac{x_{i+d} - x}{x_{i+d} - x_{i+1}} B_{i+1,d-1}(x), \tag{4}$$

and the first order spline is defined by:

$$B_{i,1}(x) = 1, x_i \le x \le x_{i+1}. \tag{5}$$

We chose to use a 3rd order polynomial curve, which means $d = 4$. Hence the Eqs. (3–5) is reduced to (assume x is scaled to [0,1]):

$$P(x) = \frac{1}{6}[x^3 \quad x^2 \quad x \quad 1] \begin{bmatrix} -1 & 3 & -3 & 1 \\ 3 & -6 & 3 & 0 \\ -3 & 0 & 3 & 0 \\ 1 & 4 & 1 & 0 \end{bmatrix} \begin{bmatrix} p_0 \\ p_1 \\ p_2 \\ p_3 \end{bmatrix}. \tag{6}$$

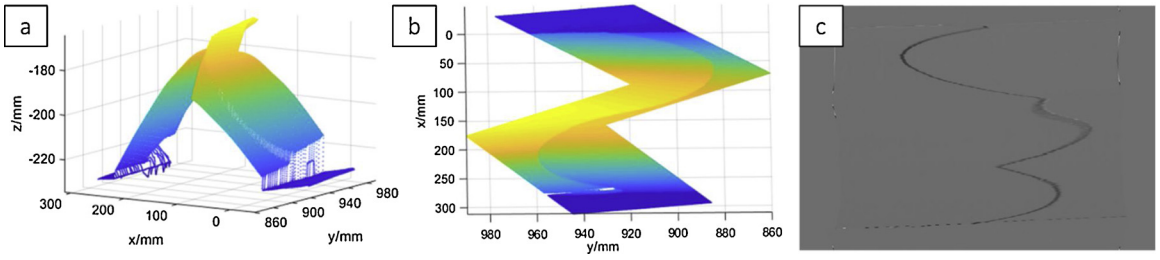

Fig. 4. Spatial weld seam image: (a, b) different views of 3D point clouds; (c) Original grayscale image.

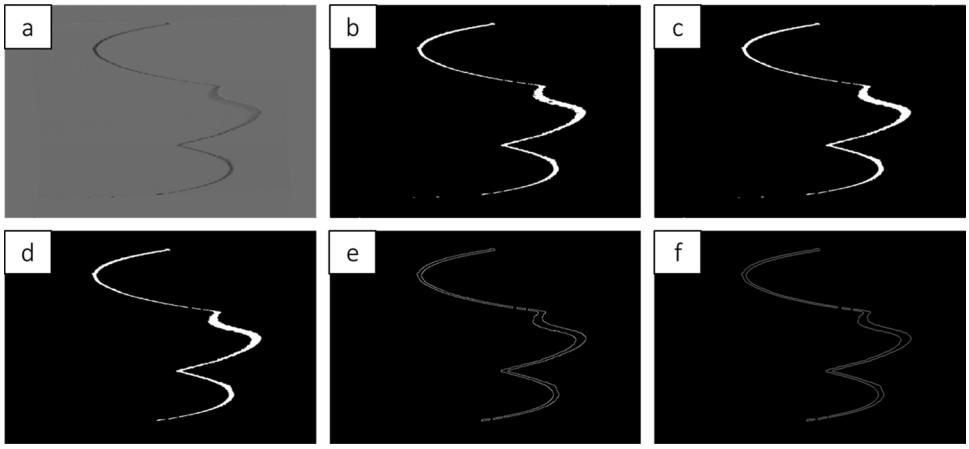

Fig. 5. Weld image processing flow: (a) Filtering and denoising; (b) Binary image by adaptive threshold segmentation; (c) Smoothing; (d) Connected domain filtering; (e) Edge detection; (f) Fine-tuning.

3.2.2. Cubic smoothing spline

A cubic smoothing spline [41] for the given data *X, Y*. The smoothing spline approximates, at the data site x_i, the given data value y_i, n is the total number of data points. This smoothing spline f minimizes:

$$S = p\sum_{i=1}^{n} |y_i - f(x_i)|^2 + (1-p)\int_{x_1}^{x_n} (f''(t))^2 dt. \tag{7}$$

The function f is a continuous cubic smoothing spline. The smoothing parameter p determines the tradeoff between smoothness and fidelity to the data. The smaller p, the smoother fitting spline; the larger p, the higher fitting accuracy.

The function f is a second-order smooth polynomial, a three-moment interpolation will be used to calculate the equations. So cubic spline f can be written as [42]:

$$f_i(x) = \frac{M_i}{6r_i}(x_{i+1}-x)^3 + \frac{M_i}{6r_i}(x-x_i)^3 + \left(\frac{y_i - d_i}{r_i} - \frac{M_i r_i}{6}\right)(x_{i+1}-x) + \left(\frac{y_{i+1} - d_{i+1}}{r_i} - \frac{M_{i+1} r_i}{6}\right),\ x_i \le x \le x_{i+1} \tag{8}$$

here, $r_i = x_{i+1} - x_i$, $i = 1, 2, \ldots n-1$. And $M_i = f''(x_i)$, $d_i = y_i - f(x_i)$, are unknown, where $i = 1, 2, \ldots n$. We adopt the natural boundary condition as: $M_1 = M_n = 0$, and for $i = 2, 3, \ldots n-1$, cubic spline interpolation $f'(x)$ meets:

$$f'(x_i - 0) = f'(x_i + 0) \tag{9}$$

From Eqs. (7–9), when S is minimized, the best relation between d_i and M_i is calculated:

$$[d_1, \ldots, d_n] = \frac{1-p}{p}[M_2, \ldots, M_{n-1}]Q \tag{10}$$

Then combining with Eqs. (8–9), the cubic smoothing spline f can be figured out.

3.3. Modeling for weld endpoints

Weld start and end points are determined by the workpiece edge line, the weld edge line and the Groove shape. The lap Groove weld endpoint detection model [43] is shown in Fig. 6, using the least squares method to fit the workpiece edge line L1, L2. Curve L3 and L4 is the part of the 3D model of weld seam, which can be obtain from methods mentioned in Section 3.2. To simplify the solution of 3D space intersection, the X-axis coordination of intersection point can be solved by lines' projection in XY plane. Then the Y, Z-axis coordination can be determined by the 3D model. Therefore, point P1, the intersection of line L2 and curve L4, is the endpoint of bottom edge of overlap seam; point P2, the intersection of line L1 and curve L3, is the endpoint of top edge of overlap seam. Results and discussion

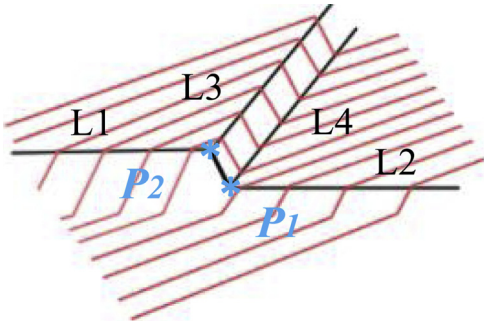

Fig. 6. Weld start and end points detection model of lap joint.

In this section, methods described in Section 3 are validated via experiments. We compared the two spatial reconstruction methods, showed 3D mold and obtained parameters of lap seam by the better method, and then verified the detected location of endpoints of spatial curve seam. The results show the validity of our proposed framework.

3.4. Comparison of two spatial reconstruction methods

The spatial reconstruction models of 3D curve welds are built by methods of cubic B-spline and cubic smoothing spline (shown in Fig. 7). Respectively, two segments of the weld where the data movement is basically consistent and the trend changes are amplified, to compare with the following modeling parameters under the modeling effect:

(a) Three B-spline curves, take one as a control point from each 5 data points, that is, $m = 5$;
(b) Cubic smoothing spline, fitting data *X, Y* by $p = 0.008145$; fitting data *X, Z* by $p = 0.0575$.

As shown in Fig. 7, the B-spline curve is more fit to the data while the smoothing spline has less curvature variation in the range (a) of fluctuating data; Both have good fitting results in range (b) where the trend of data changes smoothly. Compared with cubic smoothing spline, the B-spline has better fitting accuracy with smaller extreme and average of deviation distance (obviously shown in Fig. 8). However, Fig. 9 denotes that cubic smoothing spline has far less curvature changes which condition is closer to the actual weld seam curve.

Considering the obtained data within some inevitable noise interference, the cubic smoothing spline was adopted to model complex

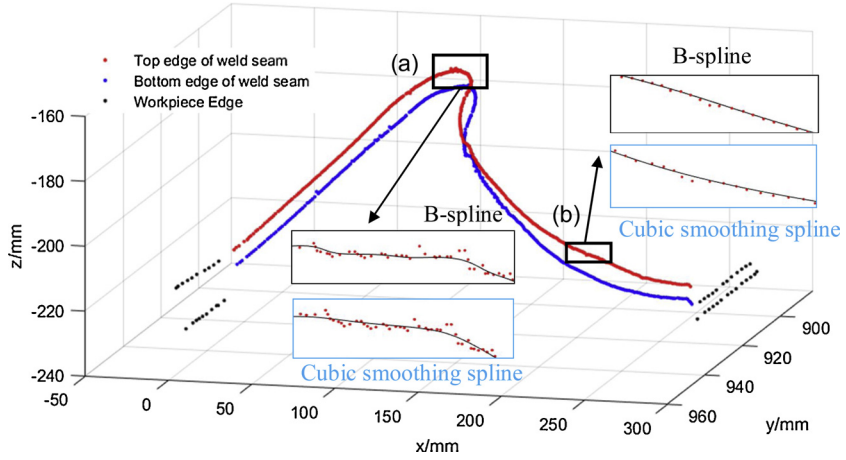

Fig. 7. Modeling contrast effect.

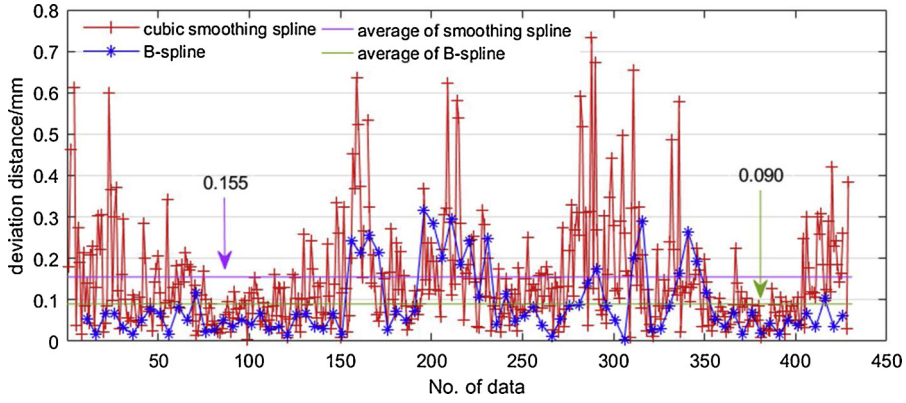

Fig. 8. Fitting deviation distance comparison.

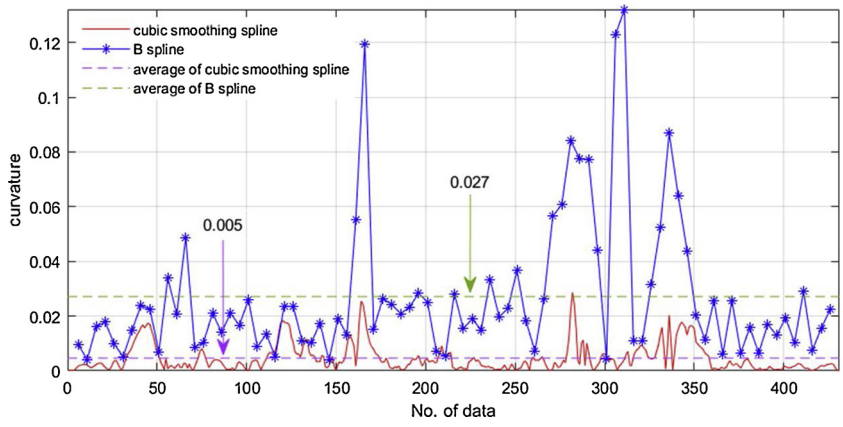

Fig. 9. Curvature comparison.

spatial curve seam and further autonomous welding because of its stronger anti-interference capability and higher curve smoothness.

3.5. Modeling and Verification of spatial curve seam

Experimental workpiece of spatial complex curve lap welding joint and its 3D model by cubic smoothing spline are shown in Fig. 10. Cubic smoothing spline curve for top edge of seam is the red curve, fitting data *X, Y* by $p = 0.008145$ and fitting data *X, Z* by $p = 0.0575$; Cubic smoothing spline curve for bottom edge of seam is the blue curve, fitting data *X, Y* by $p = 0.008145$ and fitting data *X, Z* by $p = 4.087 \times 10^{-4}$. And the 3D model basically detects the geometric feature of the lap welding seam, but still exists some deviation where the laser scanning direction changes.

By projection of data in the XY plane, the weld starting or ending point is the intersection (x, y) of two fitting lines (shown in Fig. 11), solving the X-axis coordinates and the Y, Z-axis coordination can be determined by the 3D model. Then, the coordinates of the starting and the ending points are shown in Table 2 The coordinates of the starting and the ending points. The starting and ending points of welding for lap seam are at the bottom position, which are point P_1 (-0.48, 925.56, -221.41) and point P_3 (274.18, 920.11, -227.36).

Furthermore, we can get more information about weld seam section parameters by the model above. Gap change in Z-axis direction of

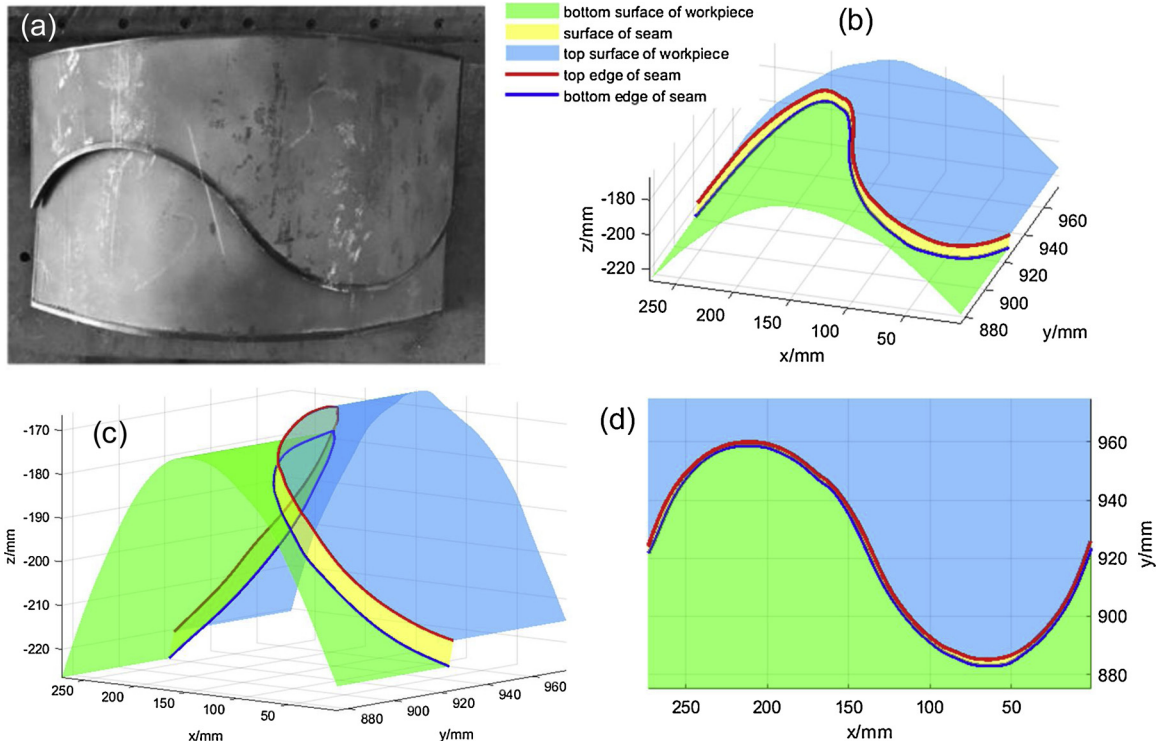

Fig. 10. Workpiece of spatial complex curve lap welding joint and its 3D model by cubic smoothing spline, a) workpiece; b, c, d) different views of its 3D model by cubic smoothing spline.

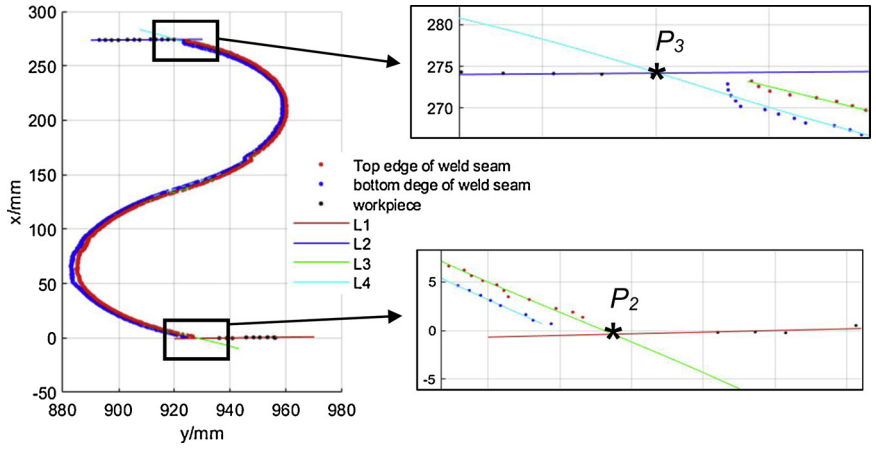

Fig. 11. Workpiece edge and weld endpoints fitting schematic.

Table 2
The coordinates of the starting and the ending points.

	x/mm	y/mm	z/mm
Starting point of bottom (P_1)	−0.484658	925.5627304	−221.4106982
Starting point of top (P_2)	−0.378036	928.7039081	−215.9206157
Ending point of bottom (P_3)	274.18415	920.1090614	−227.3585832
Ending point of top (P_4)	274.23000	922.4901262	−221.4248108

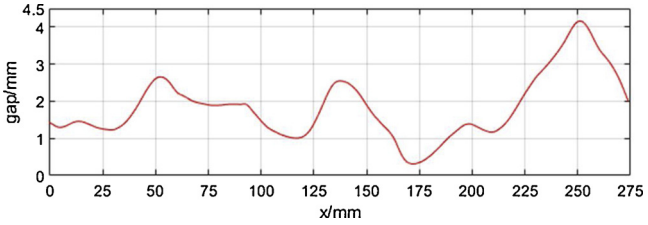

Fig. 12. Gap of complex spatial curve seam with lap joint.

complex spatial curve seam with lap joint by X- axis coordinate can be figured out: Z-axis coordinate difference value between top and bottom edge of seam at the same X-axis coordinate, minus the thickness of lap workpiece (shown in Fig. 12). And the gap change of lap seam reflects machining quality and coordination of workpiece, contributing to determination of subsequent welding process parameters.

To verify the accuracy of the 3D modeling method for lap weld recognition, the welding robot transforms 6 different posture to scan the workpiece, calculating the starting point P_1 and ending point P_3 by method proposed by this paper, 12 coordinates in total. These recognized coordinates are compared with the starting point and the ending point coordinates read by robot directly (average of three measurements). As shown in Fig. 13, No.1˜6 points represent the recognized coordinates of starting point, and No.7˜12 points are the

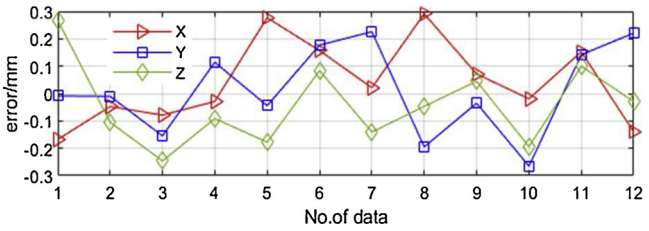

Fig. 13. Error in axis of weld starting points and ending points.

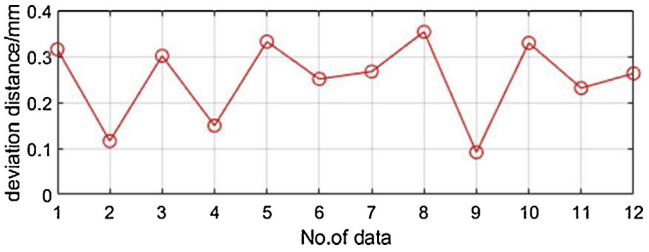

Fig. 14. Deviation distance of weld starting points and ending points.

recognized coordinates of ending point. Obviously, the error in any axis is within the ± 0.3 mm. Fig. 14 shows the distance deviation between detected endpoints and robot-read coordinates is within 0.4 mm.

Therefore, the recognition accuracy of the robotic welding system basically meeting the needs of arc welding tracking and autonomous welding. It is worth noting that the weld recognition accuracy can be improved by: replacing with the laser sensor or the industrial robot with higher precision; or modifying the calibration algorithm used, the calibration approach for linear structured light sensors which requires only a reference plate with a straight edge [35] where the max error in X, Y and Z direction is close to 0.2 mm. So that it is promising to meet higher requirements of welding condition such as laser welding, etc.

4. Conclusions

Robot welding automation and intelligence is the inevitable trend of welding technology development, this research has a practical significance to promote autonomous welding with the following three main innovations.

1 this paper introduced an autonomous welding approach based on the laser structured light sensor, which effectively obtained 3D information of large workpiece by multiple segment scanning, realized reliable 3D modeling of the complex curve weld of lap joint and detected welding endpoints with deviation lower than 0.4 mm in this experiment setup.
2 The obtained 3D point cloud data were transformed into 2D grayscale images with a height as grayscale feature, reducing the difficulty of data processing and improving the operation efficiency.
3 The reliable 3D spatial modeling of complex curve weld seam was realized by cubic smoothing spline for its stronger anti-interference capability, higher curve smoothness and better fitting to actual seam than cubic B-spline.

Acknowledgment

The authors gratefully acknowledge the financial funding of National Natural Science Foundation of China (Grants no. 51775338, 51875353, 51875354).

References

[1] Zhao W, Li S, Zhang B. Present situation and prospect of intelligent technology for welding robot. Dev Appl Mater 2016;3:108–14.
[2] You DY, Gao XD, Katayama S. Review of laser welding monitoring. Sci Technol Weld Join 2013;19(3):181–201.
[3] Nie Y, Zhang P, Zhuang Q. Key technology and research status of intelligent welding robot. Hot Work Technol 2017;46(15):7–10. 14.
[4] Muhammad J, Altun H, Abo-Serie E. Welding seam profiling techniques based on active vision sensing for intelligent robotic welding. Int J Adv Manufac Technol 2016;88(1-4):127–45.
[5] Kah P, Shrestha M, Hiltunen E, Martikainen J. Robotic arc welding sensors and programming in industrial applications. Int J Mech Mater Eng 2015;10(1).
[6] Executive Summary World Robotics. Industrial robots in. International federation of robotics, Frankfurt am Main 2017. 2017.
[7] Guo J, Zhu Z, Yu Y. Research and application of visual sensing technology based on laser structured light in welding industry. Chin J Lasers 2017;44(12). 1200001-1-01-10.
[8] Fan J, Jing F, Fang Z. Research status and development trend of welding seam tracking technology based on vision sensors. Hot Work Technol 2017;46(05). 6-10+14.
[9] Chen SB, Lv N. Research evolution on intelligentized technologies for arc welding process. J Manuf Process 2014;16(1):109–22.
[10] Chen H, Kong M, Lv N, Xu Y, Chen S. Status and development of vision sensors on intelligentized robotic welding techologies. Electr Weld Mach 2017;47(03):1–16.
[11] Meyes R, Tercan H, Roggendorf S, Thiele T, Büscher C, Obdenbusch M, et al. Motion planning for industrial robots using reinforcement learning. Procedia CIRP 2017;63:107–12.
[12] Liu Y, Zhang Y. Toward welding robot with human knowledge: a remotely-controlled approach. IEEE Trans Autom Sci Eng 2015;12(2):769–74.
[13] Liu Y, Zhang Y. Iterative local ANFIS-Based human welder intelligence modeling and control in pipe GTAW process: a data-driven approach. IEEE ASME Trans Mechatron 2015;20(3):1079–88.
[14] Chen SB, Wu J. Intelligentized methodology for arc welding dynamical processes Berlin Heidelberg 2009.
[15] Wang W, Gao X, Ding X. Study on welding seam recognition methods based on visual sensing. Hot Working Technol 2018;47(01). 195-98+202.
[16] Jin Z, Zhang C, Li H, Wang Z. Visual sensing based image processing of auto tube-sheet welding. Trans Chin Weld Inst 2017;38(10). 117-20+34.
[17] Shah HNM, Sulaiman M, Shukor AZ, Kamis Z, Rahman AA. Butt welding joints recognition and location identification by using local thresholding. Rob Comput-Integr Manuf 2018;51:181–8.
[18] Yu Z, He Y, Xu Y, Chen H. Vision-based deviation extraction for three-dimensional control in robotic welding with steel sheet. Int J Adv Manufac Technol 2018;95(9-12):4449–58.
[19] H-y Shen, Wu J, Lin T, Chen S-b. Arc welding robot system with seam tracking and weld pool control based on passive vision. Int J Adv Manufac Technol 2007;39(7-8):669–78.
[20] Kiddee P, Fang Z, Tan M. An automated weld seam tracking system for thick plate using cross mark structured light. Int J Adv Manufac Technol 2016;87(9-12):3589–603.
[21] Qiao D, Zheng J, Pan J. Dual structure laser vision sensor and its character. Electr Weld Mach 2010;40(11):14–6. 68.
[22] Zou Y, Chen T. Laser vision seam tracking system based on image processing and continuous convolution operator tracker. Opt Lasers Eng 2018;105:141–9.
[23] Huang Y, Li G, Shao W, Gong S, Zhang X. A novel dual-channel weld seam tracking system for aircraft T-joint welds. Int J Adv Manufac Technol 2016;91(1-4):751–61.
[24] Zou Y, Wang Y, Zhou W, Chen X. Real-time seam tracking control system based on line laser visions. Opt Laser Technol 2018;103:182–92.
[25] Mao Z, Zhou S, Zhao B, Shi Z, Jian Y, Pan J. Welding torch position and seam orientation deviation based on two stripes laser vision sensing. Trans Chin Weld Inst 2015;36(2).
[26] Zeng J, Chang B, Du D, Peng G, Chang S, Hong Y, et al. A vision-aided 3D path teaching method before narrow butt joint welding. Sensors (Basel) 2017;17(5).
[27] Zeng J, Chang B, Du D, Hong Y, Zou Y, Chang S. A visual weld edge recognition method based on light and shadow feature construction using directional lighting. J Manuf Processes 2016;24:19–30.
[28] Zhu J, Wang J, Su N, Xu G, Yang M. An infrared visual sensing detection approach for swing arc narrow gap weld deviation. J Mater Process Technol 2017;243:258–68.
[29] He Y, Chen Y, Xu Y, Huang Y, Chen S. Autonomous detection of weld seam profiles via a model of saliency-based visual attention for robotic arc welding. Rep U S 2015;81(3-4):395–406.
[30] Liu J, Fan Z, Olsen SI, Christensen KH, Kristensen JK. Boosting active contours for weld pool visual tracking in automatic arc welding. IEEE Trans Autom Sci Eng 2017;14(2):1096–108.
[31] Fan J, Jing F, Fang Z, Tan M. Automatic recognition system of welding seam type based on SVM method. Int J Adv Manufac Technol 2017;92(1-4):989–99.
[32] Chen X, Chen S. Recognition and positioning of start welding position for arc welding robot. Trans Chin Weld Inst 2009;30(4):17–20.
[33] Chen X, Chen S. Accuracy analysis and experimental method on three-dimensional information computing of weld seam. Trans Chin Weld Inst 2009;30(3):45–8.
[34] Chen X, Huang Y, Chen S. Model analysis and experimental technique on computing accuracy of seam spatial position information based on stereo vision for welding robot. Ind Rob Int J 2012;39(4):349–56.
[35] Zheng J, Zhang K, Luo Z, Wang Z. The hand-eye calibration of welding robot based on the constraint of spatial line. Trans Chin Weld Inst 2018;39(08). 108-113+34.
[36] Yin S, Guo Y, Ren Y, Zhu J, Yang S, Ye S. A novel TCF calibration method for robotic visual measurement system. Opt – Int J Light Electron Opt 2014;125(23):6920–5.
[37] Haralick RM, Sternberg SR, Zhuang X. Image analysis using mathematical

morphology. IEEE Trans Pattern Anal Mach Intell 1987;9(4):532–50.
[38] Leport L, Turner NC, French RJ, Barr MD, Duda R, Davies SL, et al. Physiological responses of chickpea genotypes to terminal drought in a Mediterranean-type environment. Eur J Agron 1999;11(3-4):279–91.
[39] Mallat S, Zhong S. Characterization of signals from multiscale edges. IEEE Trans Pattern Anal Mach Intell 1992;14(7):710–32.
[40] Lam L, Lee S-W, Suen CY. Thinning methodologies-a comprehensive survey. IEEE Trans Pattern Anal Mach Intell 1992;14(9):869–85.
[41] Weinert HL. A fast compact algorithm for cubic spline smoothing. Comput Stat Data Anal 2009;53(4):932–40.
[42] Zhao D, Wang L, Li Y, Du M. Extraction of preview elevation of road based on 3D sensor. Meas 2018;127:104–14.
[43] Kim P, Rhee S, Lee CH. Automatic teaching of welding robot for free-formed seam using laser vision sensor. Opt Lasers Eng 1999;31:173–82.